DIFFERENTIATION OF NOISY EXPERIMENTAL DATA FOR INTERPRETATION OF NONLINEAR STRESS-STRAIN BEHAVIOR

By Xiang-Song Li,[1] Member, ASCE, Jun Yang,[2] and Hanlong Liu[3]

ABSTRACT: Interpretation of nonlinear stress-strain behavior of a material may require differentiating the load-displacement curve constructed from experimental data. Pressuremeter and torsional shear tests in geotechnical engineering are two examples that require such an operation. Differentiating experimental data is tricky because (1) it is very sensitive to the noise inevitably existing in the measurements, and (2) the experimental data are usually only available in discrete pairs, conventional finite-difference calculations give only an approximation to the true differentiation. For these reasons, in practice the direct differentiation of experimental data is rarely performed. Instead, the experimental data are usually fitted into a particular form of mathematical function, resulting in a set of parameters representing the material behavior in an optimum sense. This paper presents a markedly different approach. The method is based on the sampling theorem and utilizes a noise-filtered differentiator to simultaneously differentiate the data and filter out the noise. The method performs true differentiation without a preassumed mathematical expression. Examples are given to show the effectiveness and limitation of this reported method.

INTRODUCTION

The data recorded during material tests are often in the form of discrete load-displacement pairs. Here, load can be a force, torque, or pressure; and the displacement can be a linear displacement, twist, or volume change. To obtain the stress-strain behavior, the recorded data need to be further interpreted. For certain types of tests, such as torsional simple shear and pressuremeter tests in geotechnical testing, due to the nonuniform strain fields in the specimens, the theoretical forms of the data interpretation involve differentiation of the recorded data. For instance, for torsional shear tests on solid cylindrical samples, based on the assumption that the shear modulus is an arbitrary function of the shear strain that varies linearly in the radial direction, Taylor (1975) derived the following interpretation equation:

$$G = \frac{2l}{\pi R^4}\left(\frac{3}{4}\frac{T}{\theta} + \frac{1}{4}\frac{dT}{d\theta}\right) \tag{1}$$

where G = secant shear modulus corresponding to the shear strain at the periphery of the sample; T = the torque applied to the sample; θ = angular displacement caused by T; and l and R = length and radius of the sample, respectively. It can be seen that to calculate G, one needs to know $dT/d\theta$.

For pressuremeter tests on clay, shear stress-strain curve can be deduced from the measured pressure-cavity strain relationship (Palmer 1972; Mair and Wood 1987) as follows:

$$\tau = \frac{1}{2}\varepsilon_c(1 + \varepsilon_c)(2 + \varepsilon_c)\frac{dp}{d\varepsilon_c} \tag{2}$$

where p = applied pressure; ε_c = measured cavity strain that is equal to one-half of the engineering shear strain γ; τ = shear stress. Again, to determine the secant shear modulus $G = \tau/\gamma$, one needs to calculate $dp/d\varepsilon_c$.

It should be pointed out that (1) and (2) are derived from elementary mechanics without considering localization issues (for instance, the gradient of angular displacement for torsional shear may vary along the sample height due to the end constraints; cracking and bifurcation may also develop at high strains). However, in consideration that (1) these two equations have many practical applications (e.g., in geotechnical tests); and (2) the scope of this paper is confined to describing a method for differentiation of noisy data rather than a discussion for data interpretation methods themselves, (1) and (2) are selected in this paper as examples to demonstrate the effectiveness and limitation of the proposed method.

Unlike differentiating a smooth mathematical function, differentiating experimental data is quite tricky. First, experimental data are inevitably scattered because of noise contamination, and by its nature the process of differentiation is extremely sensitive to the measurement noise. Second, the measured load and displacement data are usually discrete values, conventional finite-difference methods give only an approximation to the true differentiation. For these reasons, directly differentiating experimental data by the finite-difference approach may lead to erratic and even totally meaningless interpretation of the test results.

To avoid the difficulties associated with the differentiation, it is a common practice to fit the experimental data to a particular form of mathematical functions, resulting in a set of parameters representing the material behavior. Various functions have been proposed for different applications. For instance, for torsional simple shear tests the stress-strain relationships proposed by Hardin and Drnevich (1972) and Ramberg and Osgood (1943) are commonly used, the measured torque-twist data are bound to "best" fit the torque-twist relations corresponding to the proposed stress-strain relationships (Chen and Stokoe 1979). For pressuremeter tests, the measured data are fitted directly to various particular functions (e.g., Prevost and Hoeg 1975; Robertson and Ferreira 1993) and the derivatives of these functions in terms of $dp/d\varepsilon_c$ are then used to determine the shear modulus (Mair and Wood 1987).

The disadvantage of the curve-fitting approach is that the form of the mathematical expression for the material behavior is predetermined. It is evidenced by the existence of a variety of such mathematical expressions that any single expression may not be adequate to describe the nonlinear stress-strain behavior of even one material. Because the curve-fitting approach is just a numerical technique, it does not give insights into the discrepancy between the measured data and the fitted curve.

An alternative approach to differentiate the experimental

[1]Asst. Prof., Dept. of Civ. and Struct. Engrg., The Hong Kong Univ. of Sci. and Technol., Clear Water Bay, Hong Kong.
[2]Grad. Student, Dept. of Civ. and Struct. Engrg., The Hong Kong Univ. of Sci. and Technol., Clear Water Bay, Hong Kong.
[3]Res. Asst., Dept. of Civ. and Struct. Engrg., The Hong Kong Univ. of Sci. and Technol., Clear Water Bay, Hong Kong.

Note. Associate Editor. Stewart E. Swartz. Discussion open until December 1, 1998. To extend the closing date one month, a written request must be filed with the ASCE Manager of Journals. The manuscript for this paper was submitted for review and possible publication on April 11, 1997. This paper is part of the ***Journal of Engineering Mechanics***, Vol. 124, No. 7, July 1998. © ASCE, ISSN 0733-9399/98/0007-705–0712/ $8.00 + $.50 per page. Paper No. 15574.

data is examined in this paper. The method is based on the classical sampling theorem (Nyquist 1928; Shannon 1948) and utilizes a low-pass filtered differentiator to simultaneously differentiate the discrete test data and filter out the measurement noise. The method performs true differentiation (not finite difference) without a preassumed mathematical expression, for band limited data with no aliasing (it is approximately true for most practical applications), the differentiation is exact in theory. This method is highly immune from measurement noise for interpreting the behavior of a material in the medium-to-high strain range in which significant nonlinearity occurs, and because of its theoretical background, the method provides an insight into the influence of the data scattering on the deduced stress-strain relationship. This paper presents the underlying theory and the detailed algorithm of the method.

SAMPLING AND DIFFERENTIATION

The relationship between a continuous function and its discrete samples has been described by the remarkable sampling theorem uncoverd by Nyquist (1928) and Shannon (1948). In this section it is the intention of the writers to provide a background to readers who are not familiar with this subject and to show the theoretical basis of calculating derivatives of a band-limited continuous function from its discrete samples.

The sampling theorem states that if a function contains no (circular) frequency components above ω_0 in the Fourier domain, it can be completely represented by its equally spaced samples with a sampling interval $T = 2\pi/\omega_s < \pi/\omega_0$. The original function can be recovered without distortion from the sampled values by passing through an ideal low-pass filter with a bandwidth ω_f, where $\omega_0 < \omega_f < \omega_s - \omega_0$. The frequency $\omega_s/2$ is referred to as the Nyquist rate.

The basic idea of the sampling theorem is as follows. As shown in Fig. 1, a sequence of equally spaced samples $f_d(t)$ of a continuous function $f(t)$ can be viewed as the product of the function and a train of unit impulses

$$f_d(t) = f(t) \sum_{K=-\infty}^{\infty} \delta(t - KT) \tag{3}$$

in which $\delta(t - KT)$ is a Dirac delta function defined as follows:

$$\delta(t - KT) = 0, \quad t \neq KT; \quad \int_{-\infty}^{\infty} \delta(t - KT)\, dt = 1 \tag{4}$$

As a periodic function with a period $T = 2\pi/\omega_s$, the infinite-duration train of Dirac delta functions in Eq. (3) can be expressed by the following Fourier series:

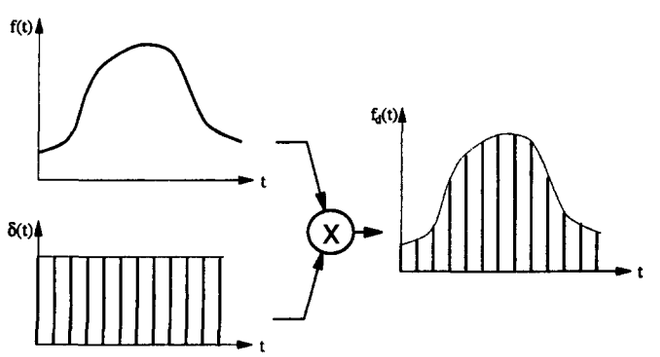

FIG. 1. Illustration of Sampling Process

$$\sum_{K=-\infty}^{\infty} \delta(t - KT) = \sum_{n=-\infty}^{\infty} \left[\frac{1}{T} \int_{-T/2}^{T/2} \sum_{K=-\infty}^{\infty} \delta(t - KT) e^{-jn\omega_s t}\, dt \right] e^{jn\omega_s t}$$

$$= \frac{1}{T} \sum_{n=-\infty}^{\infty} e^{jn\omega_s t} \tag{5}$$

hence

$$f_d(t) = \frac{1}{T} f(t) \cdot \sum_{K=-\infty}^{\infty} e^{jK\omega_s t} \tag{6}$$

and the Fourier transform of $f_d(t)$ becomes

$$F_d(j\omega) = \int_{-\infty}^{\infty} f_d(t) e^{-j\omega t}\, dt = \frac{1}{T} \sum_{K=-\infty}^{\infty} \int_{-\infty}^{\infty} f(t) e^{jK\omega_s t} e^{-j\omega t}\, dt$$

$$= \frac{1}{T} \sum_{K=-\infty}^{\infty} F[j(\omega - K\omega_s)] \tag{7}$$

Eq. (7) states that the Fourier spectrum of a sampled version of $f(t)$ is a periodic function of ω with a period of ω_s. Each period is simply a copy of each other, as shown in Fig. 2(b). It is obvious that when ω_s is greater than twice the highest frequency components ω_0 in $f(t)$, there would be no overlap-

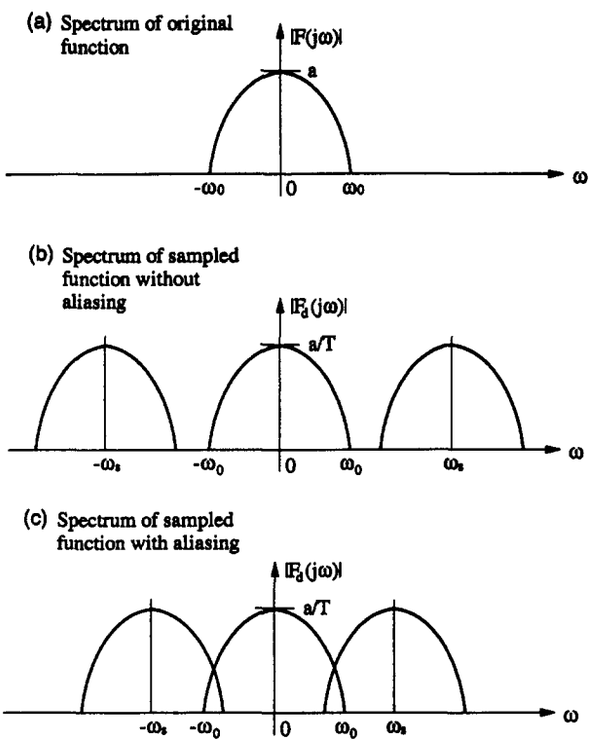

FIG. 2. Fourier Spectra of Band-Limited Continuous Function and Its Discrete Samples

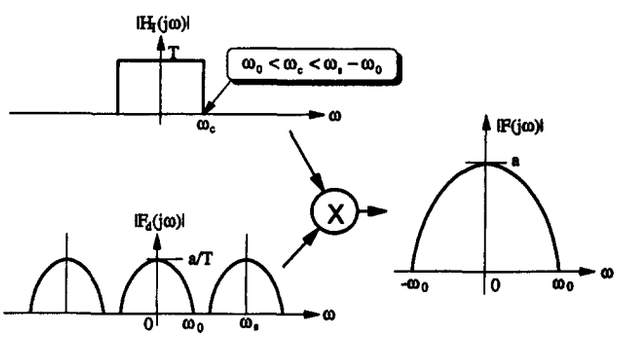

FIG. 3. Reconstruction of Continuous Function by Ideal Low-Pass Filtering

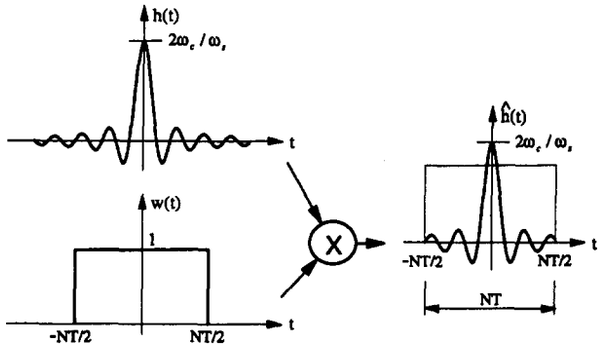

FIG. 4. Truncating Impulse Response by Windowing

ping among the periods, and each period simply contains a shifted and scaled version of the Fourier spectrum of the original function $f(t)$. Hence, the Fourier spectrum of $f(t)$, therefore, $f(t)$ itself, can be reconstructed by passing $f_d(t)$ through an ideal low-pass filter with a scaling factor T and a cutoff frequency ω_c greater than ω_0 but less than $\omega_s - \omega_0$, as shown in Fig. 3. It can be seen that $T < \pi/\omega_0$ is an inherent requirement for complete recovery of a continuous function from its equally spaced samples. If this condition is not satisfied, aliasing (evidenced by the overlapping as shown in Fig. 2c) occurs and no algorithm can cure it.

The filtering process can be described as

$$F(j\omega) = F_d(j\omega)H_I(j\omega) \tag{8}$$

where

$$H_I(j\omega) = \begin{cases} T & |\omega| < \omega_c \\ 0 & \omega_c < |\omega| \end{cases} \tag{9}$$

is the transfer function of the ideal low-pass filter with a scaling factor T and a cutoff frequency ω_c. The impulse response of the filter is the inverse Fourier transform of the transfer function, [(9)], i.e.,

$$h(t) = \frac{1}{2\pi}\int_{-\infty}^{\infty} H_I(j\omega)e^{j\omega t}\,d\omega = \frac{T}{2\pi}\int_{-\omega_c}^{\omega_c} e^{j\omega t}\,d\omega = \frac{2\sin\omega_c t}{\omega_s t} \tag{10}$$

This function is plotted in Fig. 4(a), which is symmetric about $t = 0$ and extends infinitely in both positive and negative t coordinates.

By the convolution theorem in calculus, one has

$$f(t) = \int_{-\infty}^{\infty} f_d(\tau)h(t-\tau)\,d\tau = \sum_{K=-\infty}^{\infty} f(KT)\,\frac{2\sin\omega_c(t-KT)}{\omega_s(t-KT)}$$

$$= \sum_{K=-\infty}^{\infty} f(KT)h(t-KT) \tag{11}$$

Eq. (11) serves as an interpolator for exact reconstruction of a band-limited continuous function $f(t)$ from its equally spaced samples. With (11), one may directly obtain the first derivative of f with respect to t as follows:

$$\frac{df}{dt} = \sum_{K=-\infty}^{\infty} f(KT)\,\frac{dh(t-KT)}{dt} \tag{12}$$

in which

$$\frac{dh(t)}{dt} = \frac{(2\omega_c/\omega_s)\cos\omega_c t - h(t)}{t} \tag{13}$$

has a limit 0 at $t = 0$. Eq. (12) serves as a differentiator that yields exact first derivatives of a band-limited continuous function $f(t)$ with respect to t from its equally spaced samples. Note that the derivative is expressed as a continuous function of t and may be evaluated for any given t (compare with finite-difference methods that only approximate the derivatives at discrete points). Like the interpolator, the differentiator may also be viewed as a frequency filter whose transfer function, from the properties of Fourier transform, is

$$H_D(j\omega) = \begin{cases} j\omega T & |\omega| < \omega_c \\ 0 & \omega_c < |\omega| \end{cases} \tag{14}$$

It can be seen that the differentiator has the same cutoff frequency ω_c as the one for the interpolator, implying that the differentiator does not respond to measurement noise in the frequency band beyond ω_c. In other words, (12) performs differentiation and noise filtering simultaneously, which is a welcome feature for this type of operation.

However, there is one problem in implementing these ideal filters. It can be seen from (11) and (12) that the interpolator and the differentiator are both noncausal, i.e., calculating the current value of $f(t)$ or $df(t)/dt$ needs the information in the future. An obvious solution for the problem is to approximate these ideal filters by truncating their infinite-duration impulse responses $h(t)$ and $dh(t)/dt$ to a finite duration and then to handle a delayed version of the truncated functions. This is a mature technique known as FIR (finite impulse response) filtering that has long been used in digital signal processing (Oppenheim and Schafer 1975).

Taking the interpolator as an example, for an impulse response truncated to a duration of $N \cdot T$, in which N is an integer, one has

$$f(t) \sim \hat{f}(t) = \sum_{K=I-N/2}^{I+N/2} f(KT)h(t-KT) \tag{15}$$

where the superscript "^" stands for an approximation; I = integer part of t/T. Substituting $\tau = t - N \cdot T/2$ into the preceding equation yields

$$\hat{f}(\tau) = \hat{f}\left(t - \frac{NT}{2}\right) = \sum_{K=I-N}^{I} f(KT)h\left(t - \frac{NT}{2} - KT\right) \tag{16}$$

Eq. (16) is a delayed version of (15). It can be seen that if the samples are available up to t, then $\hat{f}(t - NT/2)$ can be calculated from the available samples.

The methods commonly used in FIR filter design for generating a finite-duration impulse response to approximate an ideal response include windowing, frequency sampling, and other computer-aided approaches. A discussion on these methods is beyond the scope of this paper, readers may refer to Oppenheim and Schafer (1975) for further details. In this text only the windowing method will be introduced for its simplicity in concept and design.

As shown in Fig. 4, a truncated impulse response $\hat{h}(t)$ can be viewed as the product of the original infinite-duration response $h(t)$ and a window function $w(t)$

$$\hat{h}(t) = h(t) \cdot w(t) \tag{17}$$

in which

$$w(t) \neq 0,\ -N \cdot T/2 < t < N \cdot T/2; \quad w(t) = 0, \text{ otherwise} \tag{18}$$

where $N \cdot T$ = duration of the truncated impulse response.

By the theorem of convolution, the transfer function of a windowed filter in the Fourier domain is

$$\hat{H}(j\omega) = \frac{1}{2\pi}H(j\omega) * W(j\omega) \tag{19}$$

in which "*" = convolution operator; $H(j\omega)$ = transfer function of the filter before windowing; and $W(j\omega)$ = Fourier transform of the window function $w(t)$.

The simplest window is a rectangular one, $w_r(t)$, expressed by

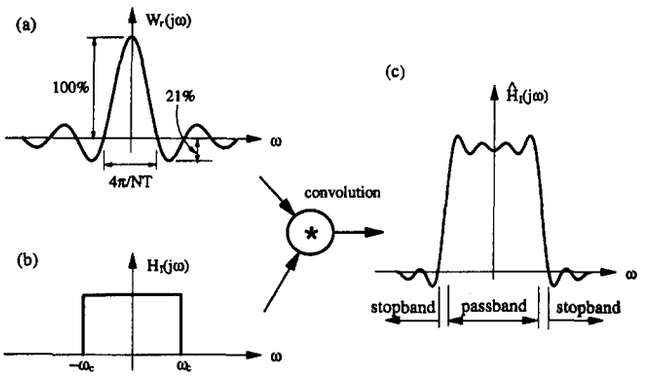

FIG. 5. Transfer Function of Rectangular-Windowed Ideal Low-Pass Filter

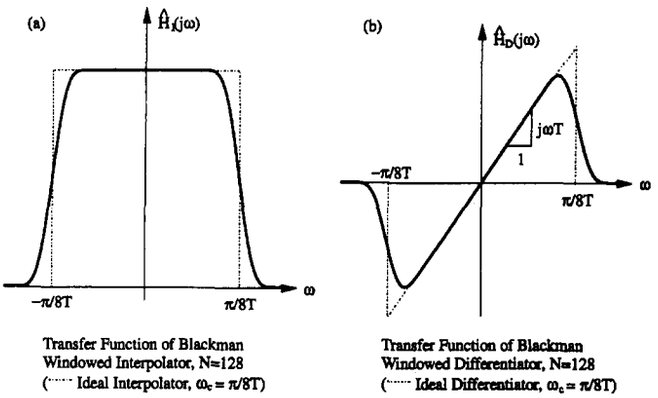

FIG. 6. Transfer Functions of Blackman-Windowed Interpolator and Differentiator

$$w_r(t) = 1, \quad -N \cdot T/2 < t < N \cdot T/2; \quad w_r(t) = 0, \text{ otherwise} \tag{20}$$

thus

$$W_r(j\omega) = \int_{-\infty}^{\infty} w(t) e^{-j\omega t}\, dt = \int_{-NT/2}^{NT/2} e^{-j\omega t}\, dt = \frac{\sin(\omega NT/2)}{\omega/2} \tag{21}$$

$W_r(j\omega)$ is shown in Fig. 5(a), which has a main lobe of width $4\pi/NT$ at the center and gradually diminished side lobes on both sides. From (19) and (21) one may calculate the transfer function of a filter whose impulse response is truncated by a rectangular window. Fig. 5 depicts this convolution process for an ideal low-pass filter (interpolator). It can be seen that, different from the ideal low-pass filter, the transfer function resulting from rectangular windowing now inserts a transition between passband and stopband. In addition to that, there are also significant unwanted "ripples" found in both the passband and stopband, particularly in the band surrounding the transition. This characteristic is referred to as Gibbs phenomenon in calculus. Fig. 5 also shows that the width of the transition band depends on the width of the main lobe and the ripples are due to the side lobes in $W_r(j\omega)$. It can also be seen from (21) that the width of the main lode and, thus, the width of the transition band, can be effectively adjusted by changing the window length NT. However, the amplitudes of the side lobes are not adjustable. For a rectangular window function, the maximum amplitude of the side lobes is about 21% of the main peak, which is considered unacceptable for most applications.

It is well-known in the theory of Fourier series that Gibbs phenomenon can be reduced at the cost of a widened transition band. An array of window functions aimed at achieving a good balance between the main lobe width and ripple amplitude have been proposed for FIR filtering, refer to Oppenheim and Schafer (1975) for a description of various window functions. The one used in this study is the well-known Blackman window given by

$$w_b(t) = \begin{cases} 0.42 + 0.5 \cos\dfrac{2\pi t}{NT} + 0.08 \cos\dfrac{4\pi t}{NT}, & -N \cdot T/2 \le t \le N \cdot T/2 \\ 0, & \text{otherwise} \end{cases} \tag{22}$$

whose transfer function is

$$W_b(j\omega) = 0.84 \frac{\sin(\omega NT/2)}{\omega} + \frac{(\omega NT)^2 \cdot \sin(\omega NT/2)}{\omega \cdot [4\pi^2 - (\omega NT)^2]} - 0.16 \frac{(\omega NT)^2 \cdot \sin(\omega NT/2)}{\omega \cdot [16\pi^2 - (\omega NT)^2]} \tag{23}$$

Because the side lobes of the superimposed components on the right-hand side of (23) are partially canceled by each other, the maximum amplitude of the side lobes of the Blackman window is less than 0.2% of the main peak. In exchange, the main lobe is widened to $12\pi/NT$.

Substituting (23), and (9) or (14) into (19) yields the transfer function of a Blackman windowed FIR interpolator or differentiator. As shown in Fig. 6, the ripples in both cases are small, within the passband the responses match the ideal filters almost exactly. This characteristic implies that, if the highest frequency component in the continuous function is within the passband, the original function and its first derivative can be recovered from its samples in a nearly exact manner.

PROCEDURE

The load-displacement relationship $L = L(D)$, as shown in Fig. 7(a), is typical for construction materials including soil. If the displacement D is considered as the dependent variable t in the previous derivation, in principle one can apply the sampling theorem and the relevant convolution techniques to interpolate and differentiate the function L. However, as L is only defined in a definite segment of D, there exist a least two problems in implementation: (1) The convolution processes for interpolation and differentiation, e.g., Eq. (16), need information outside the target segment of interest; and (2) the discontinuity of L at the ends of the defined segment of D is associated with high-frequency contents, which may increase the bandwidth of $L = L(D)$ and deteriorate the band-limited condition (hereafter the term "frequency" in this paper is referred to as the changing rate of load with respect to displacement rather than to time). To solve these problems, the following approach is used in this study.

First, the function $L(D)$ is decomposed into two functions, one linear function and one nonlinear function that vanishes at both ends of the defined segment of D as shown in Figs. 7(b) and 7(c) and is expressed as follows:

$$L(D) = L_1(D) + (a + bD) \tag{24}$$

and

$$\frac{dL(D)}{dD} = \frac{dL_1(D)}{dD} + b \tag{25}$$

where b = slope of the linear function. Because $L_1(D)$ is a continuous function possessing a finite nonzero segment, it can be converted into a periodic continuous function by alternately cloning itself and its folded and inverted copies along the D coordinate. Because the altered function in the target region of D is the same as the original one, all of the properties of $L_1(D)$ including the derivatives in this region are retained. However, because the periodic version of $L_1(D)$ is now defined for all D values, the convolution calculation such as (16) can be carried out straightforwardly. Also, because the disconti-

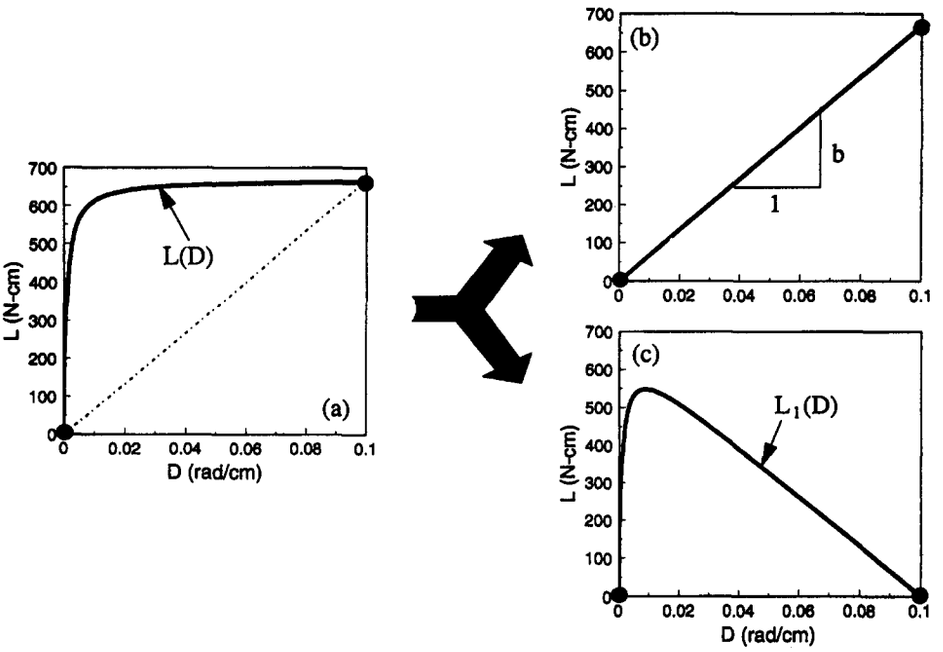

FIG. 7. Decomposition of Load-Displacement Function

nuity at the ends of the original $L_1(D)$ disappears, the high-frequency contents associated with this discontinuity also disappear.

For some nonlinear materials the material stiffness is conventionally plotted against the logarithm of strain for better visualizing the nonlinear stress-strain relationship. For example, the normalized shear modulus (G/G_{max}) of soil is almost unanimously plotted against the common logarithm of shear strain (log γ) by geotechnical engineers. Correspondingly, in tests of these nonlinear material, the data acquisition system can be conveniently programmed in such a way that the recorded data are presented with sampling intervals equal in terms of the logarithm of displacement, and the derivatives of load with respect to displacement can be easily converted from the derivatives of load with respect to the logarithm of displacement. For example, the derivative of T with respect to θ in (1) is equal to

$$\frac{dT}{d\theta} = \left(\frac{1}{\theta \cdot \ln 10}\right) \cdot \frac{dT}{d(\log \theta)} = \left(\frac{1}{2.3026 \cdot \theta}\right) \cdot \frac{dT}{d(\log \theta)} \quad (26)$$

For load-logarithm of displacement pairs of equal intervals, by treating log θ as the dependent variable, the method of calculating derivatives as described in the previous section is applicable.

In summary, the following steps are taken to calculate the derivatives of load with respect to displacement:

- Get load-displacement data pairs (e.g., T and θ) with intervals equal in displacement or in logarithm of displacement (log θ).
- Decompose the curve into a linear part and a nonlinear part $L_1(D)$. [(24)], in which D is the displacement or the logarithm of displacement (log θ), depending on the scheme of sampling intervals.
- Convert $L_1(D)$ into a periodic function by alternately cloning itself and its folded and inverted copies along the D coordinate.
- Carry out differentiation by convoluting the periodic function with a windowed differentiator [(13) windowed by (22)] over the original half period of D.
- Compose $dT/d(D)$ using (25).
- Convert $dT/d(\log \theta)$ into $dT/d\theta$ by (26) if $D = \log \theta$.

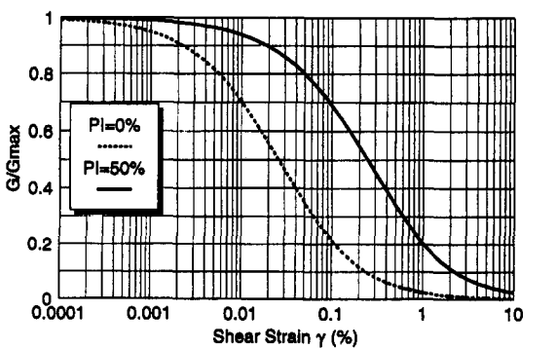

FIG. 8. Modulus Reduction Curves Used in Numerical Examples

NUMERICAL EXAMPLES

The applications of the previously described technique are illustrated by numerical examples for deriving the normalized modulus reduction curve (G/G_{max} versus γ) from two types of geotechnical tests: solid-cylinder torsional test and undrained pressuremeter tests. Eqs. (1) and (2) are the interpretation equations for the two types of tests.

Fig. 8 shows two normalized modulus reduction curves approximately following the ones proposed by Vucetic and Dobry (1991) for soils of plastic index (PI) of 0 and 50%, respectively. These two curves serve as the benchmark for checking the accuracy of data interpretation. By assuming that the change in soil stiffness depends solely on the material deformation, these two curves were first numerically converted to a load-logarithm of displacement data pairs (T − log θ and p − log ε_c for torsional shear and pressuremeter tests, respectively) as follows:

For torsional shear tests, (1) can be written as

$$\ln T - \ln T_0 = \int_{T_0}^{T} \frac{dT}{T} = \frac{2\pi R^4}{l} \int_{\theta_0}^{\theta} \frac{G(\gamma)}{T} d\theta - 3 \int_{\theta_0}^{\theta} \frac{1}{\theta} d\theta$$

$$\approx \frac{2\pi R^4 \cdot G(\bar{\gamma})}{l \cdot \bar{T}} (\theta - \theta_0) - 3(\ln \theta - \ln \theta_0) \quad (27)$$

where the shear strain $\bar{\gamma} = R(\theta + \theta_0)/2l$ is defined at the pe-

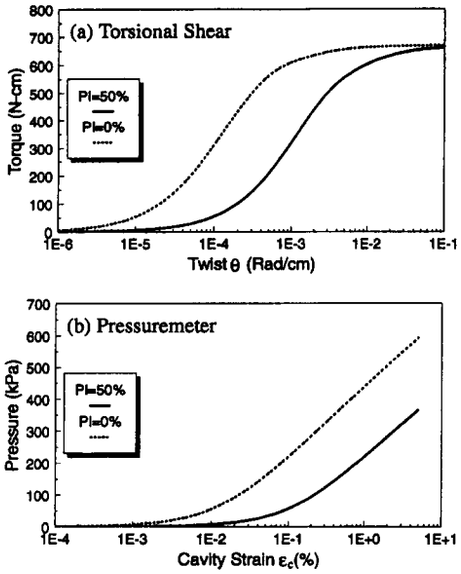

FIG. 9. Load-Displacement Curves in Numerical Examples

riphery of the sample averaged over the current loading step from θ_0 to θ; T_0 and T = torque values corresponding to θ_0 and θ, respectively; and $\bar{T} = (T + T_0)/2$ = torque value averaged over the current loading step. Starting from an arbitrarily small θ_0, where shear modulus G is independent of shear strain γ and the corresponding T_0 calculated based on linear theory, one can recursively use (27) to calculate $T - \log \theta$ pairs over the entire range of strain. In this study the loading step sizes were refined until no improvement could be seen in the $T - \log \theta$ plots. The calculated $T - \log \theta$ curves for PI = 0 and 50% are shown in Fig. 9(a)

For pressuremeter tests, (2) can be rewritten to

$$p = \int_0^p dp = \int_0^{\varepsilon_c} \frac{4 \cdot G(\gamma)}{(1 + \varepsilon_c) \cdot (2 + \varepsilon_c)} d\varepsilon_c \qquad (28)$$

with $\gamma = 2\varepsilon_c$, numerical integration can be carried out to obtain the $p - \log \varepsilon_c$ pairs. Similar to the procedure used for $T - \log \theta$ pairs, the integration step sizes were refined until no improvement could be seen. The calculated $p - \log \varepsilon_c$ curves for PI = 0 and 50% are shown in Fig. 9 (b).

With 64 pairs of discrete load-displacement samples for each of the curves covering a range of shear stains from $\sim 10^{-3}$ to 10%, the steps described in the previous section were followed to recover the normalized modulus reduction curves. In the calculation the window length $N = 1024$ [(22)] was used, and the cutoff frequency ω_c [(10) and (13)] was chosen to be ¼ of ω_s. The original and the recovered curves are plotted together in Figs. 10(a) and 10(b) for the torsional shear and pressuremeter tests, respectively. From the figures it can be seen that the recovered curves are virtually identical to their original counterparts. This verifies the principle and the procedure elaborated earlier.

While the interpretation for the modulus reduction curves was successful for noise-free load-displacement samples, its performance for noise-contaminated data must be examined. In this study, two types of additive noise were tested: (1) A sequence of random numbers generated by computer using RANDOM function, this sequence bears the characteristics of white noise; and (2) a colored noise obtained by high-pass filtering the computer generated white-noise-like sequence. The filter used was an eighth-order Butterworth filter with a normalized cutoff frequency $\pi/4$ (⅛ of sampling frequency). The noise sequences and their Fourier amplitude spectra are shown in Fig. 11. It can be seen that the type 1 noise covers the entire band (up to Nyquist frequency); therefore, it surely

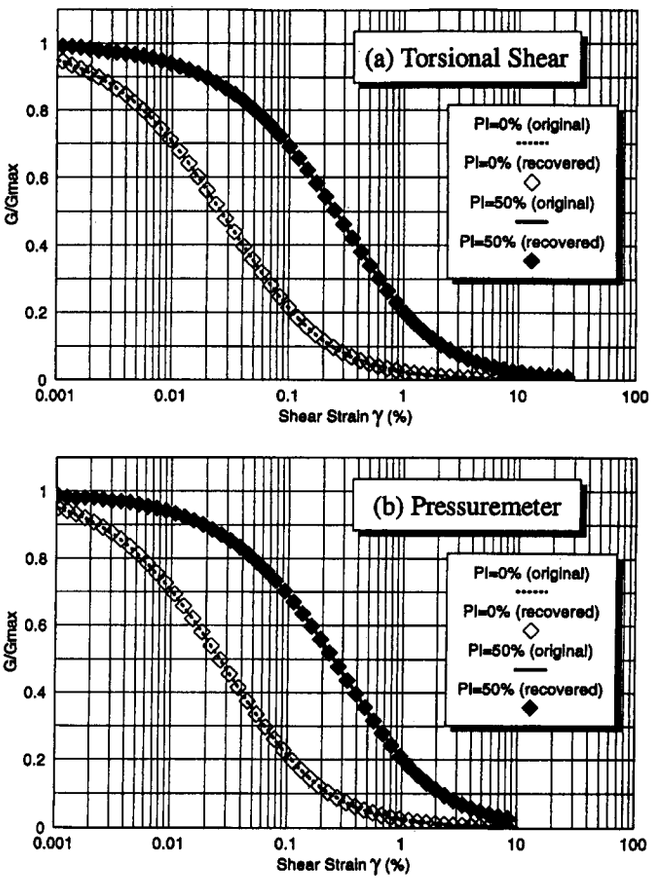

FIG. 10. Modulus Reduction Curves Recovered from Noise-Free Load-Displacement Samples

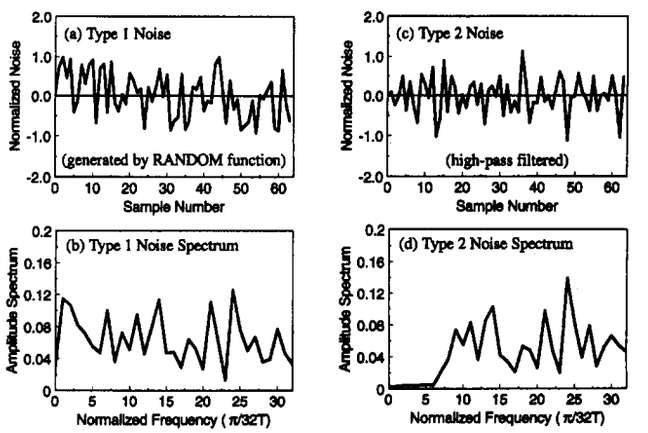

FIG. 11. Additive Noise Sequences and Amplitude Spectra

overlaps the load-displacement spectra, which implies that, once it is mixed with the load-displacement data, no filter can completely remove the noise from the latter. Numerical tests using this type of noise can show the influence of this "in-band" noise on the differentiation. For the type 2 noise, most parts of the overlapping long period components have been removed; therefore, the impact of this type of noise can be reduced by the differentiator itself because it automatically filters out high-frequency contents, as shown in Fig. 6(b). Numerical tests with this type of noise can be used to examine the effectiveness of this filtering capability. As the effects of noises added to load and to displacement are similar and convertible from each other ($\Delta L \sim [dL/dD] \cdot \Delta D$), for simplicity, the noises were added to the load samples only in this study, and the peak-to-peak amplitudes of the noises were adjusted

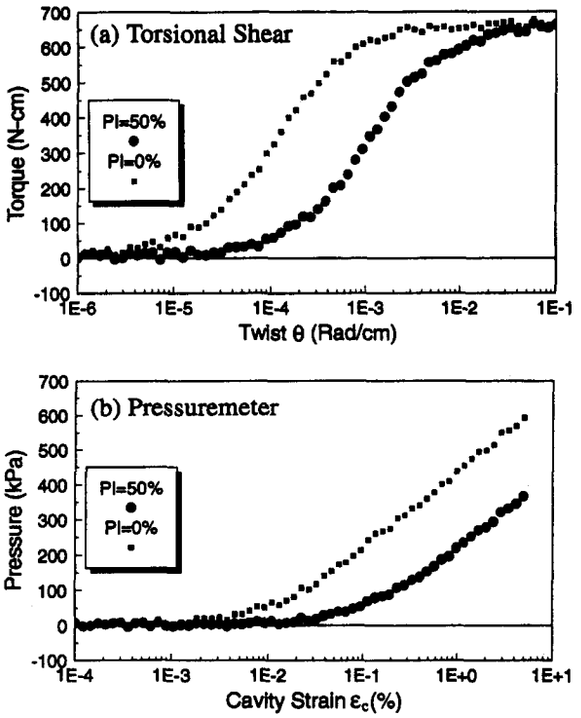

FIG. 12. Load-Displacement Curves with Type 1 Noise

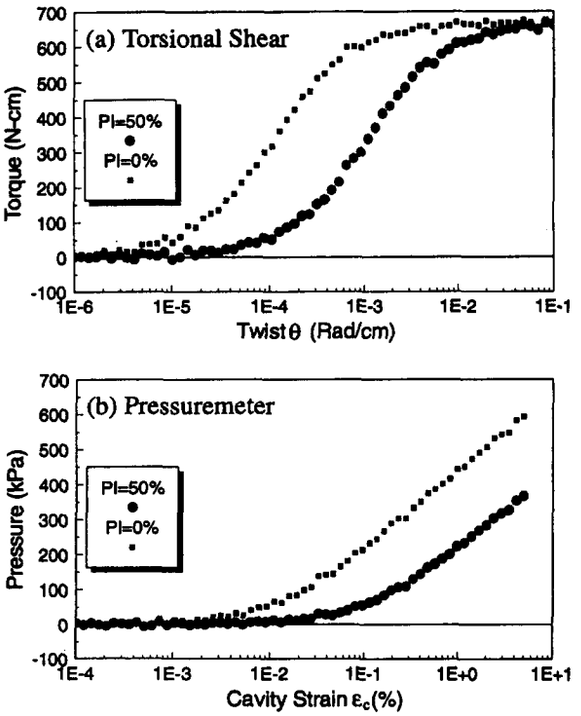

FIG. 13. Load-Displacement Curves with Type 2 Noise

to 4% of the maximum load. Figs. 12 and 13 show the load-displacement curves contaminated by the type 1 and type 2 noises, respectively. The scattering caused by the two noises are visually similar.

The normalized modulus reduction curves recovered from the noise-contaminated data are shown in Figs. 14 and 15. In the simulations the window length $N = 1024$, the cutoff frequency ω_c for the data with type 1 noise was $1/24$ of ω_s, and for those with type 2 noise was $1/12$ of ω_s. The choice of these cutoff frequences was based on the spectral characteristics of the data and noises estimated from the Fourier spectra of the noise-added load-displacement sequences. In principle, under the condition that the significant frequency contents of the load-displacement curve are retained, one would like to see ω_c be as low as possible so that the noise would be maximally eliminated. It can be seen that the curves recovered from the data contaminated by the type 1 noise are in good agreement with the original curves at shear strains higher than 10^{-2}% for PI = 0% and higher than 10^{-1}% for PI = 50%; and the curves derived from the data with the type 2 noise are good for shear strains higher than 2×10^{-3}% for PI = 0% and higher than 10^{-2}% for PI = 50%. These results show that the proposed procedure performs well in the medium-to-high strain range, where soils exhibit severe nonlinearity and the data interpretation based on linear elasticity becomes invalid.

While the characteristics and the impact of the measurement noise may vary from case to case, it is apparent that, in the very low strain range, the proposed method of differentiation may yield unsatisfactory results. However, the tests that directly measure load and displacement in a wide range of strains generally yield less reliable data at small strains, rendering the interpretation of small strain test data from such tests less important. For reliable small strain data, alternative tests such as laboratory resonant column tests (Wilson and Dietrich 1960; Drnevich et al. 1967) and geophysical tests (Stokoe and Woods 1972; Woods and Henke 1979; Stokoe and Nazarian 1985) should be carried out as a supplement. By combining the reliable small strain modulus G_{max} and the modulus reduction curve in the medium-to-high strain range, one may easily fill the gap between them either visually or using an analytical expression. In cases where the load-displacement ($L - D$) data at low strains are reliable (i.e., systematic error is low), but a little noisy, one may consider smoothing the data

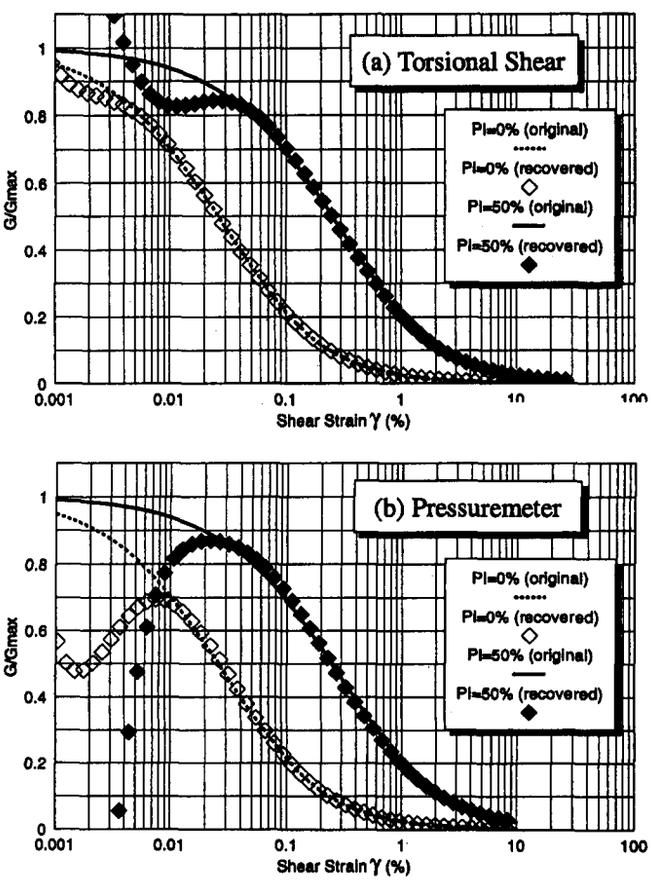

FIG. 14. Modulus Reduction Curves Recovered from Load-Displacement Samples Contaminated by RANDOM Generated "White" Noise

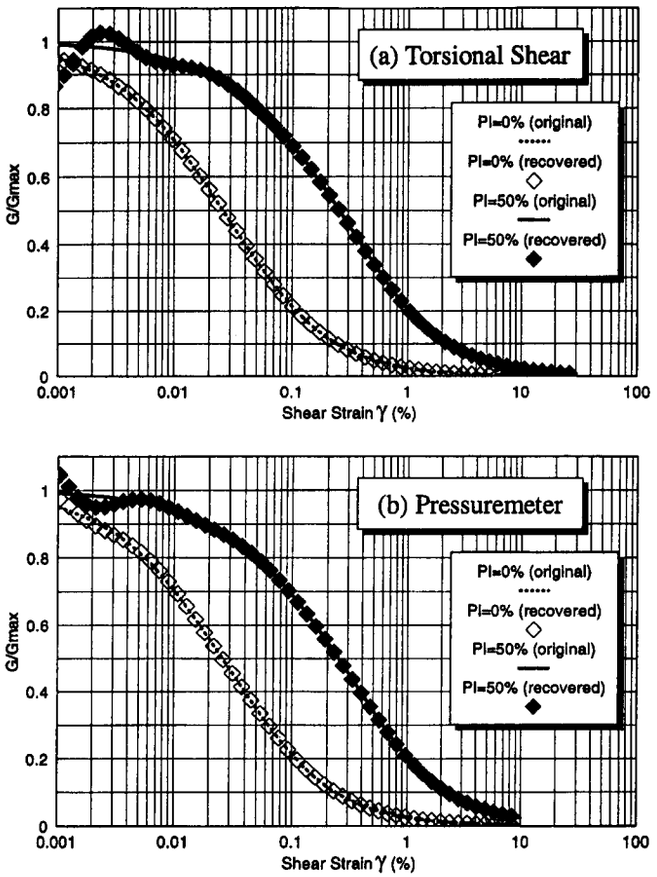

FIG. 15. Modulus Reduction Curves Recovered from Load-Displacement Samples Contaminated by High-Passed "Colored" Noise

by low-pass filtering (e.g., using the windowed interpolator introduced in this paper), and then to approximate dL/dD by L/D for the low strains, because when strain is low, the approximately linear and homogeneous relationship gives $dL/dD \approx L/D$.

SUMMARY

The interpretation of nonlinear stress-strain behavior of a material loaded under nonuniform strain fields may require differentiating the load-displacement curve constructed from experimental data. Differentiating experimental data is tricky because the data are usually discrete and noise contaminated. In this paper a procedure for differentiating discrete load-displacement data is presented. The procedure is based on classical sampling theorem and modern digital signal processing techniques. It performs true differentiation and noise filtering simultaneously. Following a brief description of the methodology and its underlying theory, applications for two types of geotechnical tests (solid cylinder torsional shear and undrained pressuremeter tests) are given for demonstration. The numerical examples show that if the load-displacement records are noise free, the procedure yields nearly exact derivatives of load with respect to displacement in both cases, resulting in almost perfect interpretations for the strain-dependent material stiffness. The procedure was then tested for load-displacement records contaminated by additive noises of different spectral characteristics. It shows that when the noises are present, the procedure works well in the medium-to-high strain range, where a valid nonlinear interpretation procedure becomes necessary.

In conclusion, the procedure presented in this paper provides an alternative way for interpreting certain types of material testing. Together with separate small strain tests, this method may yield strain-dependent material stiffness over a wide range of strains, without curve-fitting to a preassumed analytical expression.

ACKNOWLEDGMENTS

The first writer wishes to acknowledge the financial support received from the California Department of Transportation through Grant No. F92TL05 in the early stage of this work.

APPENDIX. REFERENCES

Chen, A. T. F., and Stokoe, K. H. II. (1979). "Interpretation of strain-dependent modulus and damping from torsional soil tests." U.S. Geological Survey, Menlo Park, Calif.

Drnevich, V. P., Hall, J. R., and Richart, F. E., Jr. (1967). "Effects of the amplitude of vibration on the shear modulus of sand." *Proc., Int. Symp. on Wave Propagation and Dyn. Properties of Earth Mat.*, Univ. of New Mexico Press, Albuquerque, N.M., 189–199.

Hardin, B. O., and Drnevich, V. P. (1972). "Shear modulus and damping in soils: design equation and curves." *J. of Soil Mech. and Found. Div.*, ASCE, 98(7), 667–692.

Mair, R. J., and Wood, D. M. (1987). *Pressuremeter testing.* CIRIA Ground Engrg. Rep., Butterworth's, London, England.

Nyquist, H. (1928). "Certain topics in telegraph transmission theory." *Trans. AIEE*, 47, 617–644.

Oppenheim, A. V., and Schafer, R. W. (1975). *Digital signal processing.* Prentice-Hall, Inc., Englewood Cliffs, N.J.

Palmer, A. C. (1972). "Undrained plane-strain expansion of a cylindrical cavity in clay: a simple interpretation of pressuremeter test." *Géotechnique*, London, England, 22(3), 451–457.

Prevost, J. H., and Hoeg, K. (1975). "Analysis of pressuremeter in strain softening soil." *J. Geotech. Engrg. Div.*, ASCE, 101(8), 717–732.

Ramberg, W., and Osgood, W. R. (1943). "Description of stress-strain curves by three parameters." *Tech. Note 902*, Nat. Advisory Com. for Aeronautics, Washington, D.C.

Robertson, P. K., and Ferreira, R. S. (1993). "Seismic and pressuremeter testing to determine soil modulus." *Predictive Soil Mech., Proc., Wroth Memorial Symp.*, Oxford, England, U.K., 434–448.

Shannon, C. E. (1948). "A mathematical theory of communication." *Bell Telephone Sys. Tech. Publ.*, Am. Telephone and Telegraph Co., New York.

Stokoe, K. H., and Nazarian, S. (1985). "Use of Rayleigh waves in liquefaction studies." *Measurement and use of shear wave velocity for evaluating dynamic soil properties*, R. D. Woods, ed., ASCE, Reston, Va., 1–17.

Stokoe, K. H., and Woods, R. D. (1972). "Use of Rayleigh waves in liquefaction studies." *Measurement and use of shear wave velocity for evaluating dynamic soil properties*, R. D. Woods, ed., ASCE, Reston, Va., 1–17

Taylor, P. W. (1975). "Interpretation of dynamic torsion tests on soils." *Rep. No. 120*, School of Engrg., Univ. of Auckland, Auckland, New Zealand.

Vucetic, M., and Dobry, R. (1991). "Effect of soil plasticity on cyclic response." *J. Geotech. Engrg. Div.*, ASCE, 117(1), 89–107.

Wilson, S. D., and Dietrich, D. J. (1960). "Effect of consolidation pressure on elastic and strength properties of clay." *Proc., Res. Conf. on Shear Strength of Cohesive Soils*, ASCE, Reston, Va., 419–435.

Woods, R. D., and Henke, R. (1979). "Seismic techniques in the laboratory." *Proc.*, ASCE *Geophys. Methods in Geotech. Engrg. Convention*, ASCE, Reston, Va., 293–322.